Numerical simulation of pollutant dispersion around a building complex

Mohamed Lateb[a,*], Christian Masson[a], Ted Stathopoulos[b], Claude Bédard[a]

[a] *Department of Mechanical Engineering, ÉTS (École de technologie supérieure) 1100 Notre-Dame West, Montreal, H3C 1K3 Canada*
[b] *Department of Building, Civil and Environmental Engineering, Concordia University 1455 de Maisonneuve Blvd. West, Montreal, H3G 1M8 Canada*

Abstract

The dispersion of exhausted pollutants from a building roof stack situated in the wake of a neighbouring tower has been studied using the realizable k–ϵ turbulence model and computational fluid dynamics (CFD). Two scales are considered in this work, full scale (1:1) and wind tunnel scale (1:200). Of primary interest are the distributions of the plume and of the pollutant concentrations on the building roof as well as on the leeward wall of the tower. Two stack heights and pollutant exhaust velocities have been considered to study the distribution of pollutant concentrations in the neighbourhood of the building from which the pollutant is emitted. Results are compared with measurements from field and wind tunnel experiments to estimate the accuracy of simulations.

Keywords: Numerical simulation, Computational fluid dynamics (CFD), Pollutant dispersion, Atmospheric boundary layer (ABL), Realizable k–ϵ turbulence model

1. Introduction

Increasing levels of pollution in urban environments has motivated the development of new techniques to model the dispersion of pollutants in the atmosphere. This topic is of special significance in urban areas as it is one of the significant sources of poor indoor air quality due to contamination of fresh air intakes. In the present study, the particular interest is in pollutant emissions from rooftop stacks and how the presence of the tower upstream the emitting building affects the distribution of pollutant concentrations around buildings.

Current standards for building ventilation systems recommend that rooftop stacks be designed such that their emissions do not contaminate the fresh air intakes of the emitting or any nearby buildings. Several studies have been carried out on the dispersion of pollutants in urban environments, most of which considering a single building without neighbours. Of note are the works of Mavroidis et al. (2003) who was interested in pollutant distributions around a cubic building with a transmitting continuous source of tracer gas, from different lateral and vertical positions; the research by Li and Meroney (1983a,b),who studied the concentration of exhausted pollutants from a building roof for different wind directions and stack positions; other works taking into account neighbouring structures have been carried out at wind tunnel scale. For instance, Stathopoulos et al. (2002) studied pollutant concentration, on the roof and windward wall of a building, caused by a small roof stack emitting pollutants at various speeds. Yassin et al. (2005) has reproduced a built-up area within a 500 m radius to study dispersion under various weather conditions.

Some works have been directed at improving model parameters, such as the prescription of boundary conditions or wall functions, in order to better reproduce field measurements. Among them, the

*Corresponding author. Tel.: +1 514 396 8800 ext. 7838; fax: +1 514 396 8530
Department of Mechanical Engineering, ÉTS (École de technologie supérieure)
1100 Notre-Dame West, Montreal, H3C 1K3 Canada
Email address: mohamed.lateb@etsmtl.ca (Mohamed Lateb)

work of Liu et al. (2003) focused on the use of two important parameters, namely roughness height and friction velocity, in establishing velocity and turbulence intensity profiles at the inlet of the domain. The work of Wang and Stathopoulos (2007) considered the impact of roughness height upstream of the site and on the velocity profile at the domain inlet for homogeneous and inhomogeneous terrains. Finally, Wagaman et al. (2002) carried out flow visualizations in the recirculation zones for two different building heights.

The present study considers a building in the wake of another higher building located upstream. This research complements previous experimental works completed at Concordia University in the wind tunnel and at full-scale by applying numerical modelling techniques (Computational Fluid Dynamics – CFD). The aim is to numerically reproduce experimental works of Stathopoulos et al. (2004), particularly the field experiments of August 12^{th} and 26^{th}, 2002. These experiments are simulated using the software Gambit 2.4.6 for the domain and mesh design, and Fluent 6.3.26 for the solution of the system of partial differential equations. Special attention is given to the analysis of the distribution of pollutant concentrations at various locations on the roof of the building compared to the site of the stack, while taking into account the influence of momentum ratio. The current study also provides an evaluation of the numerical approach for reproducing controlled and non-controlled experiments.

2. Numerical simulations

2.1. Model description

2.1.1. Geometric model

The geometric model consists of a building, referred to as BE, and the Faubourg tower which has the same width and four times the height of BE. The wind arrives perpendicular to the windward wall of the Faubourg tower which places the BE building in its wake. The dimensions of the BE building are $L_{BE} \times W_{BE} \times H_{BE} = 48$ m $\times$ 53 m $\times$ 12.5 m and those of the Faubourg tower are thus $L_{Fb} \times W_{Fb} \times H_{Fb} = 32$ m $\times$ 53 m $\times$ 45 m. Three structures are situated on the roof of the BE building. A penthouse is located at the back of the roof, along the downstreamwall, with dimensions 6.2 m $\times$ 18.4 m $\times$ 4 m. There is also a skylight, with dimensions 34.6 m $\times$ 6.8 m $\times$ 2.2 m, and an elevator shaft with dimensions are 10 m $\times$ 4 m $\times$ 4 m. The stack, from which the pollutant is exhausted, is at the upstream edge of the roof near the windward wall of the building. Its diameter is 0.4 m and its height varies from 1 m to 3 m. Only one structure exists at the centre of the Faubourg tower's roof with dimensions 20 m $\times$ 37 m $\times$ 5 m. Figs. 1 and 2 show the layout of these structures in plan view and elevation view, respectively. The origin of the reference frame is located at the base of thewall downstream of the BE building at its centre. Note that the wind blows in the negative x direction. Not taken into account in this geometric model are the entry of the building, located on the windward wall, and a small wall of height 1 m (parapet) that runs along the perimeter of the BE roof.

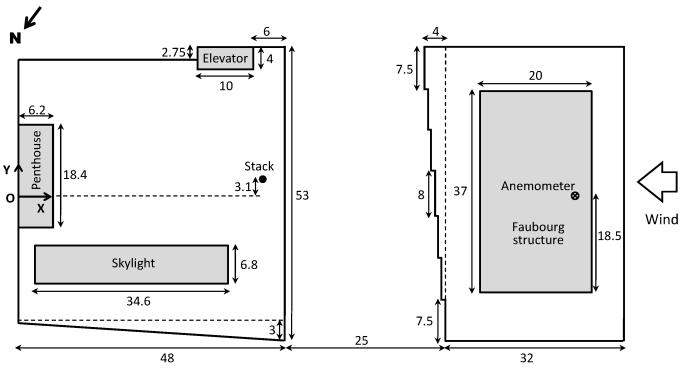

Figure 1: Plan view of the BE building and Faubourg tower. All dimensions in [m].

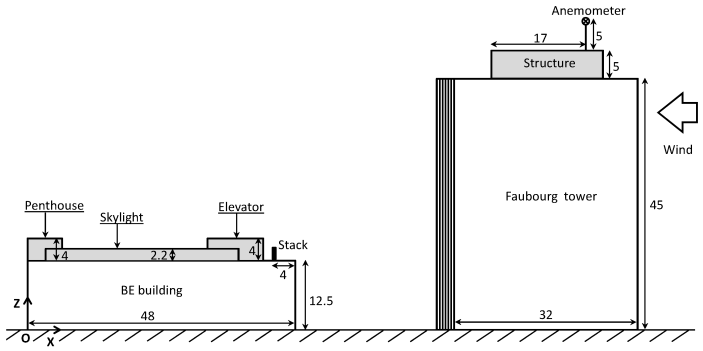

Figure 2: Elevation view of the BE building and Faubourg tower. All dimensions in [m].

2.1.2. Mathematical model

The realizable k–ϵ turbulence model is used for closure of the system of equations composed of the continuity equation, the Reynolds-Averaged Naviere–Stokes equations and an equation modelling dispersion. This choice is made following the work of Blocken et al. (2008) who studied the dispersion of pollutants around the BE building without the Faubourg tower by numerical simulation. The study concluded that the realizable k–ϵ turbulence model with enhanced wall treatment better predict the recirculation zones near the windward edge and in the wake of the building than the standard k–ϵ model. The set of equations in steady-state form are summarized below:

Equation of continuity:

$$\frac{\partial U_i}{\partial x_i} = 0 \tag{1}$$

Equation of momentum:

$$U_j \frac{\partial U_i}{\partial x_j} = -\frac{\partial}{\partial x_i}\left(\frac{\bar{P}}{\rho} + \frac{2}{3}k\right) + \frac{\partial}{\partial x_j}\left(\nu_t \frac{\partial U_i}{\partial x_j}\right) + \frac{\partial \nu_t}{\partial x_j}\frac{\partial U_j}{\partial x_i} \tag{2}$$

Equation of transport of k:

$$U_i \frac{\partial k}{\partial x_i} = \frac{\partial}{\partial x_i}\left(\frac{\nu_t}{\sigma_k}\frac{\partial k}{\partial x_i}\right) + G_k - \epsilon \tag{3}$$

Equation of transport of ϵ:

$$U_i \frac{\partial \epsilon}{\partial x_i} = \frac{\partial}{\partial x_i}\left(\frac{\nu_t}{\sigma_\epsilon}\frac{\partial \epsilon}{\partial x_i}\right) + C_1 S\epsilon - C_2 \frac{\epsilon^2}{k + \sqrt{\nu\epsilon}} \tag{4}$$

Equation of dispersion:

$$U_i \frac{\partial C}{\partial x_i} = \frac{\partial}{\partial x_i}\left(\frac{\nu_t}{\sigma_c}\frac{\partial C}{\partial x_i}\right) + S' \tag{5}$$

with:

$$\nu_t = C_\mu \frac{k^2}{\epsilon} \tag{6}$$

and: $C_\mu = \frac{1}{A_o + A_s \frac{kU^*}{\epsilon}}$; $C_1 = \max[0.43, \frac{\eta}{\eta+5}]$; $G_k = \nu_t S^2$; $\eta = S\frac{k}{\epsilon}$; $S = \sqrt{2S_{ij}S_{ij}}$; $A_s = \sqrt{6}\cos\phi$; $\phi = \frac{1}{3}\cos^{-1}\left(\sqrt{6}W\right)$; $W = \frac{S_{ij}S_{jk}S_{ki}}{\check{S}^3}$; $\check{S} = \sqrt{S_{ij}S_{ij}}$; $S_{ij} = \frac{1}{2}\left(\frac{\partial U_j}{\partial x_i} + \frac{\partial U_i}{\partial x_j}\right)$;
$\bar{P}$: Mean pressure [kg m^{-1} s^{-2}];
U_i: Mean velocity components along the three directions x, y and z [m s^{-1}];

C: Concentration of pollutant;
k: Turbulent kinetic energy [m^2 s^{-2}];
ϵ: Isotropic dissipation of turbulent kinetic energy [m^2 s^{-3}];
ν_t: Turbulent eddy viscosity [m^2 s^{-1}];
ρ: Fluid density [kg m^{-3}];
$S^{'}$: Mean volume contaminant source generation rate.

The model constants are the same as those defined in Fluent (2005): $\sigma_k = 1.0$; $\sigma_\epsilon = 1.3$; $A_o = 4.04$; $C_2 = 1.9$; $\sigma_c = 0.7$.

The pollutant concentration K is deduced after calculation by the following non-dimensional expression:

$$K = \frac{CU_H H_{BE}^2 10^{-6}}{Q_e} \tag{7}$$

with:

$$Q_e = \frac{\pi d_s^2 w_e}{4} \tag{8}$$

Q_e: Emission rate of the pollutant [m^3 s^{-1}];
C: Concentration of pollutant [ppb];
H_{BE}: Height of the BE building [m];
d_s: Diameter of the stack [m];
U_H: Velocity of the winf at the roof height of the BE building [m s^{-1}];
w_e: Exhaust velocity [m s^{-1}].

2.1.3. Numerical model

All distances were estimated taking into account the recommendations made by Tominaga et al. (2008) and Franke et al. (2007) who have proposed a set of guidelines for the CFD simulation of flows using in urban environments. The calculation domain is defined by an inlet at a distance $6.5H_{Fb}$ upstream of the Faubourg tower. This configuration was chosen to avoid perturbation of the velocity and pressure profiles in the upwind fetch due to the presence of the Faubourg tower. The domain outlet is at $11H_{Fb}$ downstream of the BE building. The lateral limits of the domain are $4.5H_{Fb}$ from each building. This choice has been made not to disturb the lateral recirculation zones caused by the Faubourg tower. The top of the domain is located at $5H_{Fb}$ from the top of the Faubourg tower.

Fig. 3 gives a global view of the grid around the building, the Faubourg tower and the structures on their roofs. A detailed grid around the stack is shown in Fig. 4. Twenty four cells are contained in the exhaust cross-section. The domain blockage ratio is 1.7%, thus it does not exceed 3% as recommended by Tominaga et al. (2008).

A structured mesh was generated with a total number of around 2.29 million cells. At the edges and the walls of the two buildings the grid is more refined as advised by several authors. Murakami and Mochida (1988, 1989) have worked particularly on 3D simulations of flow around a cube with the standard k–ϵ turbulence model. They have researched the influence of the mesh on the velocity and pressure distributions. Riddle et al. (2004) compared CFD simulations using the software Fluent and ADMS (Atmospheric Dispersion Modelling System) for atmospheric dispersion modelling. All these authors have concluded that a refined grid is able to reproduce, with good agreement, the recirculation and separation zones at edges and walls. Recently, Hefny and Ooka (2009) have investigated the effect of cell geometry on CFD results for the pollutant dispersion problem around buildings. The study compared the computational solutions of hexahedral-based and tetrahedral-based meshes at various resolutions and has concluded that the hexahedral-based mesh style provides the best computational solutions. Although meshes that employ tetrahedral elements can be constructed much faster in complex geometries, they can also increase the level of numerical diffusion. Factors that may be

considered responsible for the deterioration of grid convergence in tetrahedral-based meshes are poor mesh quality, cell non-orthogonality, skewness, and non-alignment with the predominant flow direction.

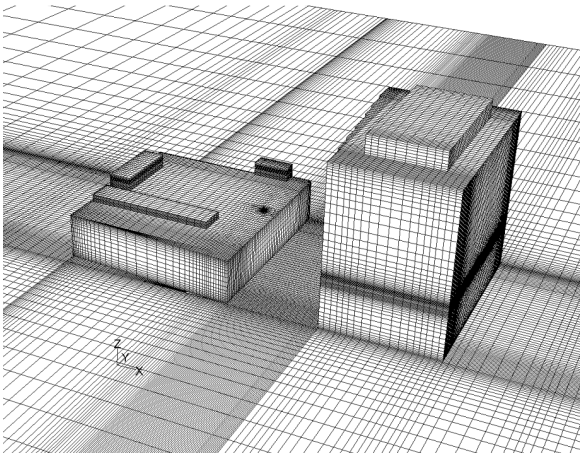

Figure 3: General view of the grid using the software Fluent.

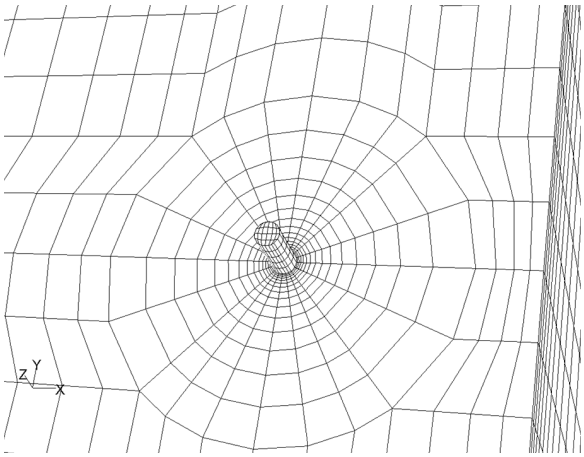

Figure 4: View of the detailed grid around the stack using the software Fluent.

In the present study, the grid is generated using software Gambit, whereas simulations are carried out with Fluent. The exit of the grid is defined as an outflow, the entry as a velocity inlet, the domain sides and top as symmetry. The segregated solver is used for getting the solution equations. The SIMPLE (Semi-Implicit Method for Pressure-Linked Equations) algorithm is used for introducing pressure into the continuity equation and QUICK scheme is used for discretizing the convection terms of momentum equation. Pressure discretization is taken care by Standard scheme. For both convection and viscous terms of the other governing equations, a second-order discretization scheme is used. The pollutant is considered a passive gas without thermal effects. As the purpose of this project is to compare results against two reports, we have chosen to take the same simulation characteristics.

2.1.3.1. Full-scale simulations. Inlet profiles are deduced from in situ measurements. The tests reproduced herein are those of Stathopoulos et al. (2004) carried out on the 12^{th} and 26^{th} of August, 2002. The wind data collected by the anemometer placed on top of the Faubourg tower (see Fig. 2) provide reference velocities U_{ref} and reference turbulence intensities TI_{ref} measured at the reference height z_{ref}.

The profiles $U(z)$ and $k(z)$ are varied at the entry until U_{ref} and TI_{ref} are obtained at the reference point. The velocity profile $U(z)$ is estimated using the power law in urban environment ($\alpha = 0.3$) :

$$\frac{U(z)}{U_{ref}} = \left(\frac{z}{z_{ref}}\right)^{\alpha} \tag{9}$$

The turbulence intensity $TI(z)$ is deduced from the equation below which relates $U(z)$ and the turbulent kinetic energy $k(z)$:

$$k(z) = \frac{3}{2}\left[U(z)TI(z)\right]^2 \tag{10}$$

The rate of dissipation of turbulent energy $\epsilon(z)$ is given by the equation:

$$\epsilon(z) = \frac{U^{*3}}{\kappa z} \tag{11}$$

with U^* obtained from the reference point situated at z_{ref} by the following equation:

$$\frac{U(z)}{U^*} = \frac{1}{\kappa} ln\left(\frac{z}{z_o}\right) \tag{12}$$

where
κ: Von Karman constant = 0.42;
z_o: Roughness length of the model (for field z_o = 0.66 m and wind tunnel z_o = 0.0033 m – see Stathopoulos et al. (2004)).

2.1.3.2. Wind tunnel scale simulations. For the reproduction of wind tunnel tests (1:200 scale), boundary conditions are derived from curves presented by Dobrescu (1994), which give the profiles of velocity and turbulence intensity at the inlet. Turbulent kinetic energy and rate of dissipation profiles have been deduced from equations (10) to (12).

The turbulence intensity TI_s of the pollutant, at its exit from the stack, is calculated from the following relation:

$$TI_s = 0.16\,(Re_s)^{-1/8} \tag{13}$$

where $Re_s = (w_e d_s \rho)/\mu$ is the stack Reynolds number and ρ and μ are the density and dynamic viscosity of the pollutant respectively.

Tables 1 and 2 list the simulation parameters used at the field and wind tunnel scales, respectively, where M is the momentum ratio, which is equal to the ratio between the exhaust velocity of the pollutant and wind velocity at height H_{BE} of the BE building. Details of vertical profiles of mean wind speed $U(z)$, turbulent kinetic energy $k(z)$, turbulence dissipation rate $\epsilon(z)$ and turbulence intensity $TI(z)$ specified at the domain entry for stack heights of 1 and 3 m are shown in the tables.

Stack height h_s [m]	Momentum ratio $M{=}w_e/U_H$	Emission rate Q_e [m^3 s^{-1}]	Turbulent intensity TI_s [%]	Profiles at the entry of the domain			
				Profile $U(z)$	Profile $k(z)$	Profile $\epsilon(z)$	Profile $TI(z)$
1	2.3	0.96	3.45	$1.56 \times z^{0.3}$	$0.47/z^{0.4}$	$0.391/z$	$0.3588/z^{0.5}$
	4.9	1.98	3.16	$1.51 \times z^{0.3}$	$0.39/z^{0.4}$	$0.352/z$	$0.3998/z^{0.5}$
3	1.7	0.86	3.50	$1.90 \times z^{0.3}$	$0.62/z^{0.4}$	$0.716/z$	$0.3383/z^{0.5}$
	3.9	1.93	3.17	$1.85 \times z^{0.3}$	$0.54/z^{0.4}$	$0.653/z$	$0.3236/z^{0.5}$

Table 1: Simulation parameters used at field scale (1:1).

Stack height $200h_s$ [m]	Momentum ratio $M{=}w_e/U_H$	Emission rate $\times 10^{-5}$ Q_e [m^3 s^{-1}]	Turbulent intensity TI_s [%]	Profiles at the entry of the domain			
				Profile $U(z)$	Profile $k(z)$	Profile $\epsilon(z)$	Profile $TI(z)$
1	2.2	4.36	6.2	$14.5 \times z^{0.3}$	$1.25/z^{0.4}$	$2.17/z$	$0.063/z^{0.5}$
	5	9.91	5.6				
3	2.2	4.36	6.2				
	4.5	8.92	5.7				

Table 2: Simulation parameters used at wind tunnel scale (1:200).

2.2. Error evaluation

In the present study, two different types of errors have been evaluated. The first kind concerns inlet profile inhomogeneity and the second discretization errors due to cell sizes. To analyse inhomogeneity, the streamwise evolution of inlet profiles in an empty domain (mean wind speed U, turbulent kinetic energy k, turbulence dissipation rate 3 and turbulence intensity TI) have been plotted at 200 m intervals starting from the inlet. For the other case, the influence of the number of cells on the simulation results has been evaluated.

2.2.1. Inhomogeneity error

Recently, many researchers have studied the presence of inhomogeneity in the simulated atmospheric boundary layer. Yang et al. (2005) concluded that it is important as a precondition for numerical simulation to evaluate the quality of the simulated equilibrium boundary layer. Blocken et al. (2007) also suggested that it is advisable to assess the effects of horizontal inhomogeneity by performing a simulation in an empty computational domain. In this work, the error related to inhomogeneity is evaluated as suggested by Blocken et al. (2007) and the results obtained are comparable to that work.

2.2.2. Grid refinement error

Celik et al. (2008) detailed a procedure for the estimation of uncertainty due to discretization in CFD applications. The study recommended a 5-step process: define a representative cell, select three significantly different sets of grids, calculate the apparent order, determine the extrapolated values and evaluate the estimated errors. The fine grid convergence index (GCI) has been calculated with the averaged relative error of the parameter of interest; in this case, the concentration K at several samplers. For the evaluation of the grid refinement error, three grids were selected with a total number of 1.59, 1.99 and 2.29 million cells, respectively. The process is detailed below.

The definition of a representative cell or mesh size l for threedimensional problems is:

$$l = \left[\frac{1}{N} \sum_{i=1}^{N} \Delta v_i \right]^{\frac{1}{3}} \tag{14}$$

where Δv_i is the volume of the ith cell and N is the total number of cells used in the grid. The grid refinement factor r is defined as the ratio of representative coarse cell size to representative fine cell size, illustrated by the following equation:

$$r = \frac{l_{coarse}}{l_{fine}} \tag{15}$$

Many researchers recommend using a minimal value of this factor between 1.1 and 1.3; the smaller value being sufficient to differentiate the discretization error from the sources of error like iterative convergence error or computer round-off error.

The relative error in K, at each sampler, between the coarse and fine resolutions is given by:

$$e = \left| \frac{K_{i,coarse} - K_{i,fine}}{K_{i,fine}} \right| \tag{16}$$

and the average relative error e_a for all the concentrations K_i obtained at all samplers and for all simulations with the same grid is calculated as follows:

$$e_a = \frac{1}{J} \sum_{i=1}^{N} e_i \tag{17}$$

where J is the total number of concentrations collected from all samplers for the same grid resolution (with any height and momentum ratio). The grid convergence index (GCI) then indicates, as a percentage, how far the computed value is from the asymptotic value. This gives an idea of how the variables of interest would change with further grid refinement.

$$GCI = F\frac{e_a}{r^p - 1} \tag{18}$$

with F as a safety factor and p as the order of the discretization method (if the systems of interest are based on second-order discretization of all terms in space, then $p = 2$). The F value used is 1.25, as suggested by Celik et al. (2008). Table 3 gives the details of the computational cases used for this grid refinement study.

Scale simulation	Total number of cells [$\times 10^6$]	Grid refinement factor value r	Average relative error e_a[%]	Grid convergence index GCI [%]
1:1	1.99 vs 2.29	1.05	0.64	7.78
	1.59 vs 1.99	1.08	9.55	71.74
1:200	1.99 vs 2.29	1.05	1.06	12.92
	1.59 vs 1.99	1.08	8.72	65.49

Table 3: Calculation details of the grid refinement error.

Through the current analysis of discretization error, it appears that the lowest values of e_a and GCI are obtained for the two successively finer grids at both simulation scales. At field scale the lowest average error and grid convergence index are about 0.64% and 7.78%, respectively, which are lower than those found at wind tunnel scale. This means that the two finer grids for the field scale simulations give concentration values relatively closer to each other than those obtained in the wind tunnel simulations, in the case of the average relative error. For the grid convergence index, the percentage value, at field scale, is again smaller than that found at wind tunnel scale. It can be concluded that for the field scale simulations, with the two successively more refined grids, the solution changes less in relative terms than it does at wind tunnel scale. To obtain comparable values from the wind tunnel simulations, it would be necessary to further refine the grid.

As the concentrations K obtained for the two successive refined grids are so close, the errors obtained are acceptable and further grid refinement would significantly increase processing time with only negligible increase in accuracy. Therefore, 2.29 million cells were used for the remainder of the study. Please note that the obtained Y^+ values near the walls are in the range of 2–5.

3. Numerical results and validation

The experiments of Stathopoulos et al. (2004) were used to validate the numerical model. These experiments were carried out, in fullscale, on the roof of a 3-storey building which used to house the Department of Building, Civil and Environmental Engineering at Concordia University in downtown Montreal. The building is situated 25 m away from a 12-storey tower located on its southwest side. The field tests were carried out in strong winds ($U_{Dorval} > 4$ m s^{-1}) according to measurements taken at Dorval airport provided by Environment Canada. The wind arrives from the south-west and places the BE building in the wake of the Faubourg tower. Wind speeds of this magnitude correspond, according to classes defined by Pasquill, to a neutral or slightly unstable atmosphere and lend themselves well to wind tunnel modelling according to Stathopoulos et al. (2004).

The wind tunnel tests were carried out at the boundary layer wind tunnel of Concordia University. The models of the BE building, Faubourg tower, and surroundings were reproduced at 1:200 scale. In

the windward direction, the surroundings were reproduced up to a distance of 250 m. In the leeward direction, the neighbouring buildings were included up to a distance of 50 m.

The results of the field and wind tunnel experiments carried out by teams at IRSST (Institut de Recherche Robert-Sauvé en Santé et Sécurité du Travail) and at Concordia University, respectively, have allowed comparisons of concentrations obtained at different samplers located on the leeward wall of the Faubourg tower and on the emitting building roof, for configurations of interest with different stack heights and exhaust velocities of pollutant.

In the present study, numerical results obtained at each scale are presented and compared to their corresponding experimental values.

3.1. Full-scale simulations

Fig. 5 presents the K distribution on the BE roof and leeward wall of the Faubourg tower, for a stack height of 1 m and for a momentum ratio of 2.3. The majority of K values obtained are overestimated at most sampler locations. Only those on the windward part of the roof and in close vicinity of the stack are underestimated. The underestimation average error is about 62%. On the leeward wall of the Faubourg tower, K is underestimated at sampler F_{B1} whereas at sampler F_{B3} it is overestimated. This is due to the staircase shape of the leeward facade which does not permit a symmetric dispersion of the pollutant in this part between the two buildings. The highest overestimation errors are found at samplers R_{35} and R_{25} located at the south-east corner of the BE roof.

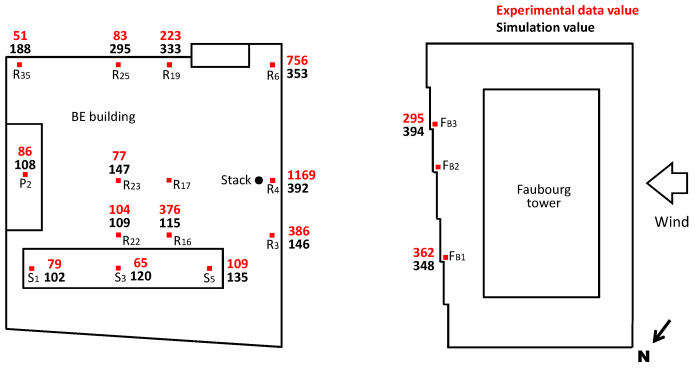

Figure 5: Simulation (1:1 scale) and field values for K ($M = 2.3$ and $h_s = 1$ m).

Fig. 6 also presents the distribution of K, but for a momentum ratio of 4.9 with the same stack height. Again, almost all samplers on the BE roof overestimate K. Only in the close vicinity of the stack is K underestimated, as in the previous case. On the leeward wall of the Faubourg tower, overestimation is also observed. However, a reduction in the underestimation of K around the stack (R_3 and R_4) with increased exhaust velocity was noted. The highest average error of overestimation remains at sampler R_{25}. Overall, the increase in exhaust velocity produces a smaller zone around the stack where K is underestimated, and increases the overestimation of K at the centre of the south-east wall, particularly at samplers R_{25} and R_{19}. For sampler R_6, located at the south corner of BE building, the effect is completely reversed.

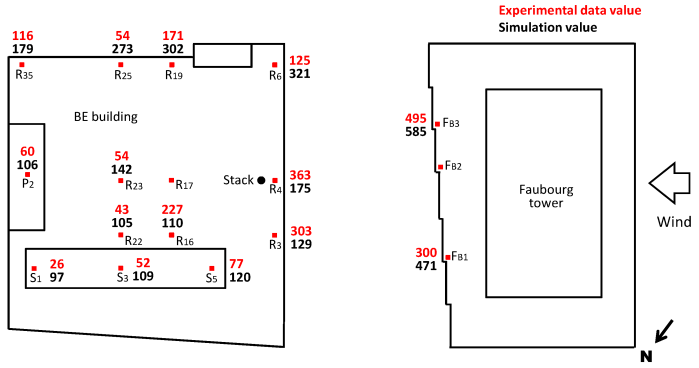

Figure 6: Simulation (1:1 scale) and field values for K ($M = 4.9$ and $h_s = 1$ m).

Fig. 7 presents a comparison of K values between field tests and full-scale simulations for three samplers (R_4, R_{23} and P_2) along the x (stack) axis and for two different exhaust velocities. The underestimation of the simulated K values noted before, in Fig. 5 at sampler R_4, is clearly shown on this figure. For $M = 2.3$, the measured concentration is three times higher than the calculated value at sampler R_4. But, for a momentum ratio twice greater ($M = 4.9$), the field value is just two times that of fullscale simulations. Better results for this case were expected: doubling the emission velocity should increase the turbulence intensity, the dispersion near the stack and consequently K at the sampler R_4. However the computed value at $M = 4.9$ is still lower than that obtained for $M = 2.3$. Clearly, the dispersion is not well reproduced despite the increase in velocity. The same observation has been made by Stathopoulos et al. (2004) in their work.

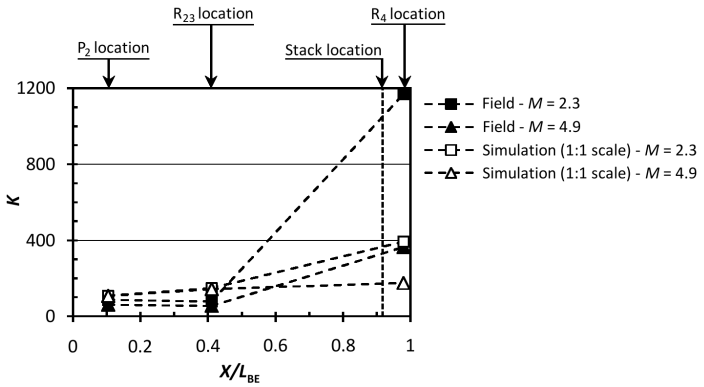

Figure 7: Measured and computed (1:1 scale) variation of K along x axis on BE roof ($h_s = 1$ m).

Fig. 8 presents the vertical distribution of K along the leeward wall of the Faubourg tower upwind of the stack. Here, simulations significantly overestimate K. The calculated distributions for the lower half of the Faubourg tower have the same form as their measured counterparts and the overestimation is roughly constant for this region although very significant. In contrast, the simulated K profile varies in reverse fashion with respect to the field profile for the upper half. The overestimation decreases to its smallest value at the top of the Faubourg tower. The pollutant plume does not appear to be as well evacuated vertically as observed in the field experiment. Consequently, the major part of the pollutant is transported to the lower half and makes the K values overestimated. Since similar evolutions of K are observed in the lower half region for both measurements and simulations, flow recirculation occurring in the lower half region seems to be well reproduced.

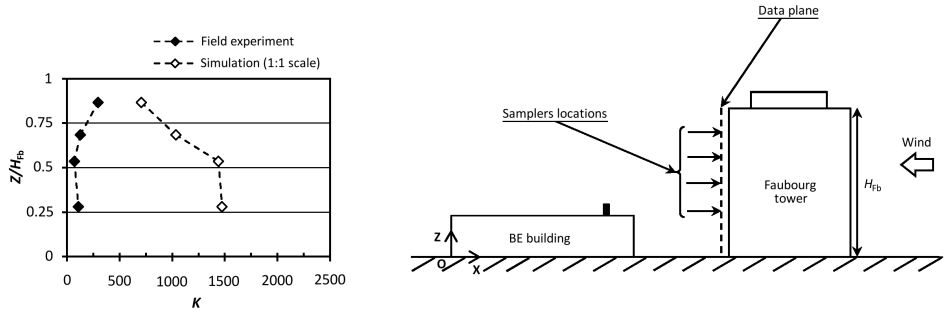

Figure 8: Vertical profiles of K on leeward wall of Faubourg tower (Field and simulation 1:1 scale values, $M = 3.9$ and $h_s = 3$ m).

The dispersion of K values between field tests and simulations at full-scale is given in Fig. 9a and b. On the BE roof (Fig. 9a), the majority of samplers have overestimated K, only 21% of them are underestimated. Forty percent of values are positioned within a range of factor 2, as indicated by points situated between the lines on each side of the median line. For the samplers located at the top of the Faubourg leeward wall (F_{B1}, F_{B2}, and F_{B3}) all values are within a factor of 2 and overestimation is still the dominant tendency (Fig. 9b).

To summarize, simulation values overestimate, at most samplers, the concentrations compared to those recorded in the field. An underestimation on the windward part of the BE roof is observed and it is more important around the stack for low pollutant velocity. Doubling the pollutant exhaust velocity produces a significant decrease of the underestimation in this region. Far from the stack, at the roof centre, the variation with exhaust velocity is less important than around the stack. The pollutant plume is not sufficiently evacuated vertically and the flow seems to be correctly reproduced in the lower part between the two buildings, but not in the upper part. The dispersion around the stack appears to be poorly predicted, even for the high exhaust velocity case. Probably, the existence of the parapet in the field experiments imprisons the pollutant at samplers located in the windward zone of the roof and particularly at sampler R_4. This parapet is not simulated in CFD, so it can be the origin of poor prediction in this area.

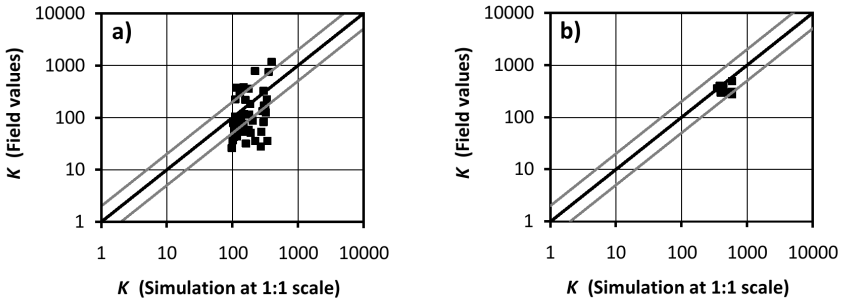

Figure 9: Scatter plots of simulation (1:1 scale) and field K data. (a) On the BE roof and (b) on the Faubourg leeward wall.

3.2. Wind tunnel scale simulations

Figs. 10 and 11 present experimental and simulation values of K at the wind tunnel scale for a stack height of 1 m and for $M = 2.2$ and 5, respectively. For moderate exhaust velocity (Fig. 10), almost half of samplers have overestimated K and the majority of them are situated along the south-eastwall of the BE roof and on the skylight structure. The sampler R_4 near the stack also overestimates K, but

this is the only sampler located along the centre region of the roof which does so. Most of the others have underestimated K by a factor less than 2.

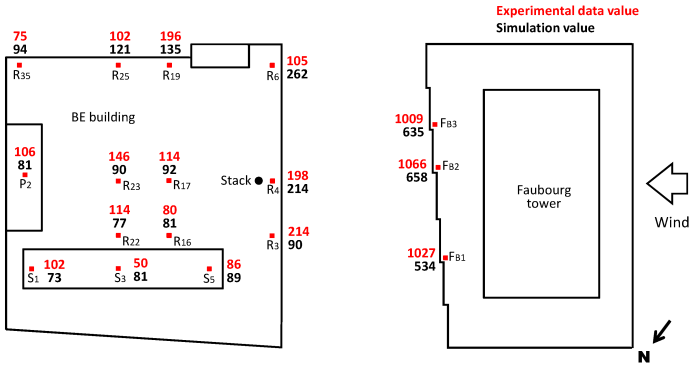

Figure 10: Simulation (1:200 scale) and wind tunnel values for K ($M = 2.2$ and $h_s = 1$ m).

For higher pollutant velocities (Fig. 11), the calculated concentration at most samplers increases and surpasses those measured in the wind tunnel experiments. Only at samplers in close vicinity to the stack as well as F_{B1} and R_{19} K is still underestimated.

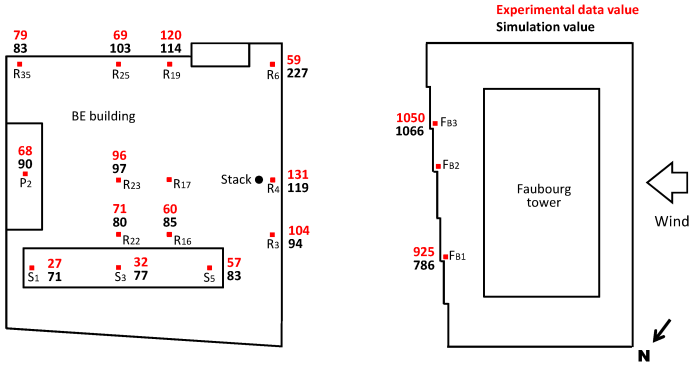

Figure 11: Simulation (1:200 scale) and wind tunnel values for K ($M = 5$ and $h_s = 1$ m).

Comparing Fig. 12, at wind tunnel scale (1:200) with Fig. 7 at full-scale, it is clear that simulations at wind tunnel scale are in better agreement with measurements for samplers located near the stack and BE roof centre. As pollutant concentrations decrease away from the stack, the conclusions of Stathopoulos et al. (2004) that the leeward wall of the BE building, for this configuration, is the best side to install fresh air intakes are confirmed.

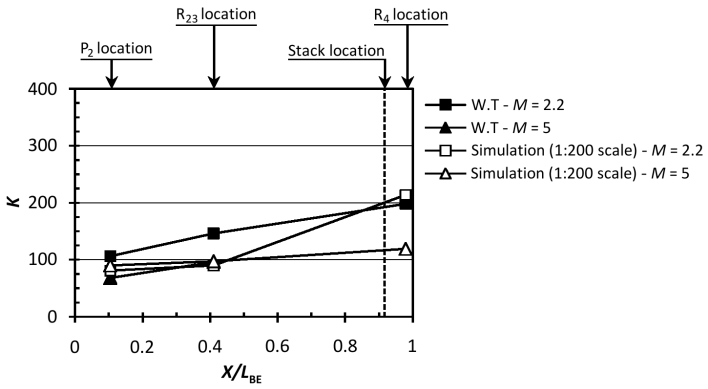

Figure 12: Measured and computed (1:200 scale) variation of K along x axis on BE roof ($h_s = 1$ m).

Similar to Fig. 8, Fig. 13 presents the vertical distribution of concentrations along the leeward wall of the Faubourg tower. An overestimation is also noted for this simulation, but less significant than for the full-scale simulation. Distributions of K again have the same form in the lower half of the Faubourg tower but are reversed in the upper half. The closest values are again reached at the top of the Faubourg tower. The results obtained at the two scales are comparable, but overestimation is larger at field scale.

In the case of simulations at wind tunnel scale with $h_s = 3$ m and $M = 4.5$, the peak of K along the downstream wall of the Faubourg tower is at mid height. This is explained by the fact that the pollutant plume is evacuated upwards from the stack directly towards the leeward wall of the Faubourg tower and it is separated thereafter in two directions: one ascending and one descending; as it moves away from the impact point, the concentration decreases.

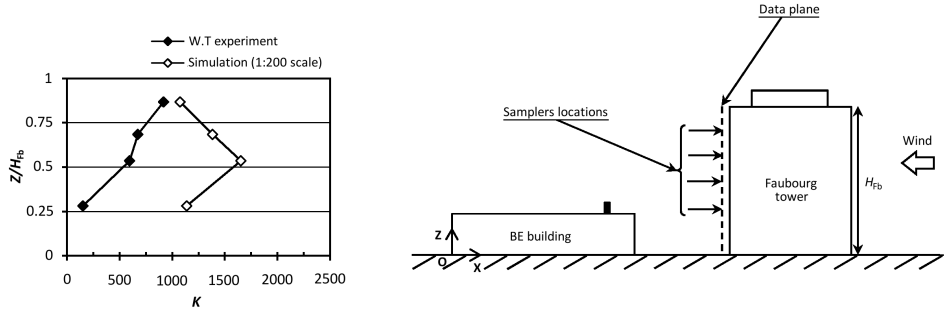

Figure 13: Vertical profiles of K on leeward wall of Faubourg tower (Wind tunnel and simulation 1:200 scale values, $M = 4.5$ and $h_s = 3$ m).

As already observed in full-scale simulation, the pollutant plume does not appear to be as well evacuated vertically. Thus the general trends of pollutant concentration are well captured in the lower region, but not in the upper; and it is likely that recirculation has not been well reproduced above the mid height of the Faubourg tower.

Fig. 14a compares the dispersions of K values on the BE roof between wind tunnel experiments and CFD simulations at 1:200 scale. Eighty percent (80%) of concentration values are situated within a range factor of 2, with 30% of K values being underestimated. For results obtained on the leeward wall of the Faubourg, as shown in Fig. 14b, the same is observed and all K values are within a range factor of two. But in this case, 80% of results underestimate the measured K values contrary to field scale simulations where overestimation is the dominant tendency.

Wind tunnel simulation results show an overestimation of K values around the stack and in the

south-east region of the BE roof. A small underestimation is noted at the other sampler locations on the roof. A more pronounced underestimation is observed on the leeward wall of the Faubourg tower. Increasing the pollutant exhaust velocity reduces the difference between experimental and simulated concentrations, except at sampler R_6. The flow field is better reproduced in the lower part between the two buildings compared to the region above the mid height of the Faubourg tower.

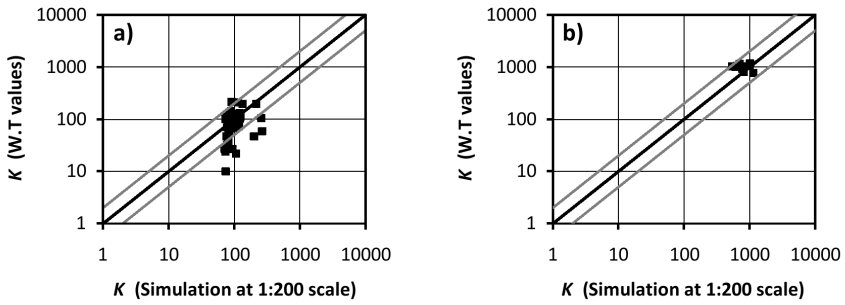

Figure 14: Scatter plots of simulation (1:200 scale) and wind tunnel K data. (a) On the BE roof and (b) on the Faubourg leeward wall.

3.3. Summary of simulation results

Differences between measured and calculated concentrations, at almost all sampler locations on the BE roof and Faubourg leeward wall, are more pronounced at field scale than at wind tunnel scale. At samplers located on the south-east wall (R_{35}, R_{25} and R_{19}), the variation of K with stack height and exhaust velocity is different than at other samplers on BE roof. The upstream flow coming around the Faubourg tower finds a broader opening on the side of sampler F_{B1}. This results in greater dilution on this side, thus driving a major part of the pollutants towards the south-east zone. Consequently, concentration at samplers located on that part of the BE roof increases. It is possible that the large differences in concentrations between simulations and experimental results are due to the presence of a neighbouring building which has not been included in the numerical model. Irrespective of this, overestimations are less pronounced at the wind tunnel scale.

At samplers located on the Faubourg tower leeward wall, simulation values of K overestimate field scale data, while for wind tunnel scale simulations, results underestimate experimental values. The pollutant plume is not sufficiently transported vertically in simulations than it has been observed in experimental tests. For both scales, the vertical variation of concentration values shows that the flow between the two buildings has not been correctly reproduced in the upper half of the tower. However in the lower half, it seems to be correctly simulated.

Finally, simulations at wind tunnel scale have better reproduced the corresponding experimental values than at field scale. This is likely due to the highly controlled environment under which wind tunnel tests are performed.

4. Error analysis

The average error is calculated, using the equation below, over all samplers and for each stack height and exhaust velocity. Its variation as a function of momentum ratio for each stack height is shown in Fig. 15a and b for field and wind tunnel scales, respectively. The standard deviation is also included for each case.

$$e_a = \frac{1}{n}\sum_{i=1}^{n}\left|\frac{K_{i\ sampler,simulation(N\ cells)} - K_{i\ sampler,exp}}{K_{i\ sampler,stack\ exit}}\right| \tag{19}$$

with:
e_a: Average relative error of all samplers;
$K_{i\ sampler,exp}$: Concentration measured experimentally;
$K_{i\ sampler,stack\ exit}$: Concentration obtained numerically at the centre stack exit;
$K_{i\ sampler,simulation(N\ cells)}$: Concentration obtained numerically using a grid with N cells.

With respect to Fig. 15a, the average error and standard deviation are lowest for small exhaust velocities and tall stack heights at field scale. At wind tunnel scale, shown in Fig. 15b, the best results are obtained at high exhaust velocity and with the lowest stack height. Comparing the two figures, wind tunnel simulations better reproduce experimental results than field scale simulations, as already mentioned.

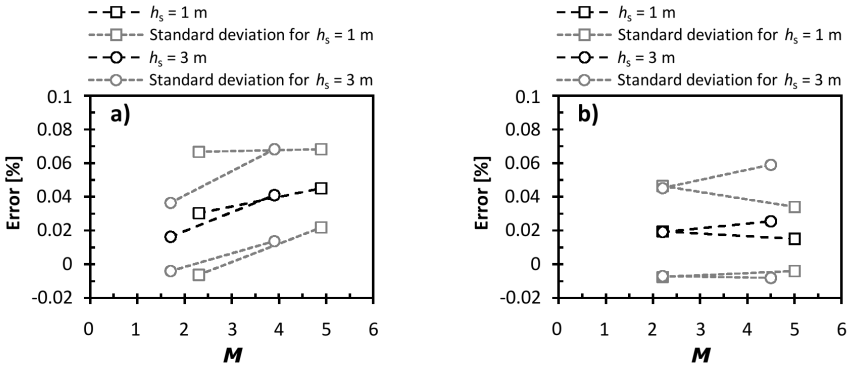

Figure 15: Average error between measured and calculated k for different M and h_s values. (a) Measured ans calculated at (1:1 scale) and (b) at (1:200 scale).

5. Conclusion

This work investigates the dispersion of pollutants emitted from a roof stack in the wake of a tower in urban environment. Numerical simulations are carried out with the realizable k–ϵ turbulence model. Two scales are considered, namely full-scale (1:1) and wind tunnel scale (1:200). During this study, the primary interest is to reproduce field and wind tunnel experiments by calculating the distributions of pollutant concentrations in the vicinity of a building with a roof stack, for two different stack heights and exhaust velocities.

As a result of this work, conclusions can be summarized as follows:

- Simulation results at full-scale (1:1) underestimate pollutant concentrations at samplers located around the BE roof stack and overestimate them everywhere else. The increase in exhaust velocity produces a smaller zone around the stack in which K is underestimated and increases the overestimation of K in the south-east part of the roof.
- Wind tunnel scale (1:200) CFD simulations tend to underestimate the values measured in wind tunnel experiments (particularly along the centre region of the roof and at leeward samplers of the Faubourg tower) except around the stack and on the south-east side of the BE roof. Increasing the exhaust velocity generally reduces differences in K values; however, the opposite tendency is observed around the stack and on the south-east part of the Faubourg leeward wall (due to the staircase shape of the leeward facade). The relative errors are rather low compared to those at field scale.
- The calculated average errors for all K values show that results of wind tunnel scale simulations are closer to experiment than those at field scale. This clearly brings light on the numerical approach capability to reproduce experiments in controlled and non-controlled environments.
- At both scales, CFD simulations did not well reproduce the wake zone observed in the experiments. The lower region between the two buildings seems to be correctly reproduced, resulting in

the same trends of pollutant concentrations. However the upper half has not been correctly simulated resulting in a pollutant plume which is not sufficiently elevated vertically when compared to the experiment observations.

- The leeward wall of the BE building remains the best side to install fresh air intakes for this building with the configuration considered.

Acknowledgements

Financial support for this study from the *Fonds Québécois de la Recherche sur la Nature et les Technologies* (*FQRNT*) is gratefully acknowledged. The authors would like also to express their special appreciation to the *Institut de Recherche Robert-Sauvé en Santé et Sécurité de Travail* (*IRSST*) team of Montreal, Canada for their cooperation.

References

Blocken, B., Stathopoulos, T., Carmeliet, J., 2007. Cfd simulation of the atmospheric boundary layer: Wall function problems. Atmospheric Environment 41 (2), 238–252.

Blocken, B., Stathopoulos, T., Saathoff, P., Wang, X., 2008. Numerical evaluation of pollutant dispersion in the built environment: Comparisons between models and experiments. Journal of Wind Engineering and Industrial Aerodynamics 96 (10–11), 1817–1831.

Celik, I. B., Ghia, U., Roache, P. J., Freitas, C. J., Coleman, H., Raad, P. E., 2008. Procedure for estimation and reporting of uncertainty due to discretization in CFD applications. Journal of Fluids Engineering 130 (078001), 1–4.

Dobrescu, M. A., 1994. Effect of mismatching model and boundary layer scales in estimating pollutant dispersion around buildings. M.A.Sc Thesis, Department of Building, Civil and Environmental Engineering, Concordia University, Montreal, Canada.

Fluent, 2005. Fluent 6.3 User's Guide, Fluent Inc., Lebanon.

Franke, J., Hellsten, A., Schlünzen, H., Carissimo, B., 2007. Best practice guideline for the CFD simulation of flows in the urban environment. Cost Action 732.

Hefny, M., Ooka, R., 2009. CFD analysis of pollutant dispersion around buildings: Effect of cell geometry. Building and Environment 44 (8), 1699–1706.

Li, W. W., Meroney, R. N., 1983a. Gas dispersion near a cubical model building: Part I. Mean concentration measurements. Journal of Wind Engineering and Industrial Aerodynamics 12 (1), 15–33.

Li, W. W., Meroney, R. N., 1983b. Gas dispersion near a cubical model building: Part II. Concentration fluctuation measurements. Journal of Wind Engineering and Industrial Aerodynamics 12 (1), 35–47.

Liu, G., Xuan, J., Park, S., 2003. A new method to calculate wind profile parameters of the wind tunnel boundary layer. Journal of Wind Engineering and Industrial Aerodynamics 19, 1155–1162.

Mavroidis, I., Griffiths, R. F., Hall, D. J., 2003. Field and wind tunnel investigations of plume dispersion around single surface obstacles. Energy and Buildings 37 (21), 2903–2918.

Murakami, S., Mochida, A., 1988. 3-d numerical simulation of airflow around a cubic model by means of the k–ϵ model. Journal of Wind Engineering and Industrial Aerodynamics 31, 283–303.

Murakami, S., Mochida, A., 1989. Three-dimensional numerical simulation of turbulent flow around buildings using the k–ϵ turbulence model. Building and Environment 24 (1), 51–64.

Riddle, A., Carruthers, D., Sharpe, A., McHugh, C., Stocker, J., 2004. Comparisons between FLUENT and ADMS for atmospheric dispersion modelling. Atmospheric Environment 38, 1029–1038.

Stathopoulos, T., Lazure, L., Saathoff, P., Gupta, A., 2004. The effect of stack height, stack location and rooftop structures on air intake contamination: A laboratory and full-scale study. In: Report R-392. Institut de recherche Robert-Sauvé en santé et en sécurité du travail (IRSST), Montreal, Canada, IRSST/Report-392.

Stathopoulos, T., Lazure, L., Saathoff, P., Wei, X., 2002. Dilution of exhaust from a rooftop stack on a cubical building in an urban environment. Atmospheric Environment 36 (29), 4577–4591.

Tominaga, Y., Mochida, A., Yoshie, R., Kataoka, H., Nozu, T., Yoshikawa, M., Sharasawa, T., 2008. AIJ guidelines for practical applications of CFD to pedestrian wind environment around buildings. Journal of Wind Engineering and Industrial Aerodynamics 96 (10–11), 1749–1761.

Wagaman, S. A., Rainwater, K. A., Mehta, K. C., Ramsey, R. H., 2002. Full-scale flow visualization over a low-rise building. Journal of Wind Engineering and Industrial Aerodynamics 90, 1–8.

Wang, K., Stathopoulos, T., 2007. Exposure model for wind loading of buildings. Journal of Wind Engineering and Industrial Aerodynamics 95, 1511–1525.

Yang, W., Quan, Y., Jin, X., Tamura, Y., Gu, M., 2005. Influences of equilibrium atmosphere boundary layer and turbulence parameter on wind loads of low-rise buildings. Journal of Wind Engineering and Industrial Aerodynamics 96 (10–11), 2080–2092.

Yassin, M. F., Kato, S., Ooka, R., Takahashi, T., Kouno, R., 2005. Field and wind-tunnel study of pollutant dispersion in a built-up area under various meteorological conditions. Journal of Wind Engineering and Industrial Aerodynamics 93 (5), 361–382.